HydrothermalFoam v1.0: a 3-D hydro-thermo-transport model for natural submarine hydrothermal systems

Zhikui Guo[1,2], Lars Rüpke[2], and Chunhui Tao[1,3]

[1]Key Laboratory of Submarine Geosciences, MNR, Second Institute of Oceanography, MNR, Hangzhou 310012, China
[2]GEOMAR Helmholtz Centre for Ocean Research Kiel, Wischhofstr. 1-3, 24159 Kiel, Germany
[3]School of Oceanography, Shanghai Jiao Tong University, 1954 Huashan Rd., Shanghai 200030, China.

Correspondence: Lars Rüpke (lruepke@geomar.de) and Chunhui Tao (taochunhuimail@163.com)

Abstract. Herein, we introduce *HydrothermalFoam*, a three dimensional hydro-thermo-transport model designed to resolve fluid flow within submarine hydrothermal circulation systems. *HydrothermalFoam* has been developed on the OpenFOAM platform, which is a Finite Volume based C++ toolbox for fluid-dynamic simulations and for developing customized numerical models that provides access to state-of-the-art parallelized solvers and to a wide range of pre- and post-processing tools. We have implemented a porous media Darcy-flow model with associated boundary conditions designed to facilitate numerical simulations of submarine hydrothermal systems. The current implementation is valid for single-phase fluid states and uses a pure water equation-of-state (IAPWS-97). We here present the model formulation, OpenFOAM implementation details, and a sequence of 1-D, 2-D and 3-D benchmark tests. The source code repository further includes a number of tutorials that can be used as starting points for building specialized hydrothermal flow models. The model is published under the GNU General Public License v3.0.

1 Introduction

High temperature hydrothermal circulation through the ocean floor plays a key role in the exchange of mass and energy between the solid earth and the global ocean (German and Seyfried, 2014; Elderfield and Schultz, 1996). It influences the thermal evolution of young oceanic plates (Stein and Stein, 1994; Theissen-Krah et al., 2016), modulates global ocean biogeochemical cycles (German et al., 2016; Tagliabue et al., 2010), and is associated with massive sulfide ore deposits that form around vent sites (Hannington et al., 2011). Hydrothermal convection occurs over large spatial and temporal scales. At fast spreading ridges, convection cells may either be confined to the upper extrusive crust above the axial melt lens (Faak et al., 2015; Coumou et al., 2008; Fontaine et al., 2009), or extend all the way down to the crust mantle boundary at approx. 6 km depth (Hasenclever et al., 2014; Dunn et al., 2000; Cathles, 1993). At slow spreading ridges, fluid circulation may extend much deeper (up to 35 km) into the ultramafic mantle (Schlindwein and Schmid, 2016), although the maximum extent of the brittle layer remains debated and may be confined to the upper 15 km (Grevemeyer et al., 2019). Such deep-reaching fluid flow can sometimes be channelized along deep detachments at fault-controlled systems such as TAG and Lonqi (Tao et al., 2020; deMartin et al., 2007) and/or may propagate to greater depths via thermal cracking (Olive and Crone, 2018; Lister, 1974). Temperatures can also vary over large ranges with high-temperature systems typically being driven by a magmatic heat source of 1000 °C or more and

porosity/permeability staying open up to 600 - 800 °C (Lister, 1974). Finally, hydrothermal systems can evolve over long times scales of up to 50-100 kyrs (Jamieson et al., 2014) but also respond to shorter events like glacial sealevel changes (Middleton et al., 2016) or magmatic as well as seismic events (Germanovich et al., 2000; Wilcock, 2004; Singh and Lowell, 2015) and even tidal pressure changes (Crone et al., 2011; Barreyre et al., 2018). These spatial and temporal scales in combination with the extreme pressure (P) and temperature (T) conditions (up to 300 MPa and 1000 °C) of submarine hydrothermal systems make direct and long-term observations challenging and pose a problem for laboratory work (Ingebritsen et al., 2010). Hence, numerical simulations have become indispensable tools for understanding and characterizing fluid flow and for relating seafloor observations to physico-chemical processes at depth.

In the last decades, significant progress has been made in hydrothermal flow modelling both theoretically and numerically (Lowell, 1991; Ingebritsen et al., 2010). Due to the high complexity of the heterogeneous sub-seafloor, a continuum porous medium approach based on Darcy's law is typically used, in which the conservation equations are written for control volumes with effective properties such as Darcy velocity, permeability, and porosity. Such approaches have been successfully used to make fundamental progress in our understanding of the nature and mechanisms of hydrothermal transport, including a thermodynamic explanation of black smoker temperatures (Jupp and Schultz, 2000), the three-dimensional structure of hydrothermal circulation cells at mid-ocean ridges (Coumou et al., 2009; Hasenclever et al., 2014), and phase separation phenomena as well as salinity variations of hydrothermal fluids (Lewis and Lowell, 2009a, b; Coumou et al., 2009; Weis et al., 2014).

Current numerical simulators of hydrothermal flow can be divided into two families: 1) multi-phase codes that thrive towards resolving saltwater convection and associated phase separation phenomena and 2) single-phase hydrothermal codes that focus on sub-critical low-temperature fluid flow and/or super-critical high-temperature flow of pure water, i.e. codes that only "work" within single-phase fluid states. Multi-phase saltwater codes are at the forefront of what is currently feasible in numerical simulations as accounting for the complexity of the equation-of-state (EOS) of seawater (Driesner and Heinrich, 2007; Driesner, 2007) in combination with multi-phase transport is a challenge (Ingebritsen et al., 2010). Existing codes of this type include CSMP++, which is capable of treating salt water up to magmatic temperatures on unstructured finite element-finite volume (FEFV) meshes (Weis et al., 2014). The hydrothermal multi-phase version of CSMP++ is currently 2-D and it's a closed-source project. FISHES is a 2-D open-source academic code, which uses the finite volume method to solve thermohaline convection on structured meshes (Lewis and Lowell, 2009a, b) but has some restrictions on the phase states that can be resolved. Currently there is no 3-D model that can resolve multi-phase saltwater convection but there are some developments efforts on the way. In addition, there are a number of geothermal modeling codes that can handle two-phase behavior that have not (yet) been adapted to handle the complex EOS of saltwater over sufficiently large pressure and temperature ranges. HYDROTHERM (Kipp et al., 2008), FEHM (Zyvoloski et al., 1997), HT2_NR (Vehling et al., 2018), and TOUGH2 (Pruess et al., 1999) are examples of such codes. The second type of code family refers to somewhat simpler models that circumvent the numerical challenges of multi-phase phenomena by staying in P-T regions, where the simulated fluid is in single-phase. A popular approach is to use a pure water instead of a saltwater EOS at pressures beyond the critical end-point (22 MPa). These models, despite making simplifying assumptions, continue to be widely used in the submarine hydrothermal system community and have been successfully applied to solve a wide range of problems. Examples include Jupp and Schultz (2000, 2004), who showed that hydrothermal systems

60   operate close to optimal efficiency with their maximum vent temperatures set by the thermodynamic properties of water, studies that revealed the complex 3-D structure of recharge and discharge flow in mid-ocean ridge hydrothermal systems (Hasenclever et al., 2014; Coumou et al., 2008; Fontaine et al., 2014), dedicated case studies for individual vent systems (Tao et al., 2020; Andersen et al., 2015; Lowell et al., 2012), and models exploring tidal forcing of hydrothermal circulation (Crone and Wilcock, 2005; Barreyre et al., 2018). This list is nowhere near complete and there are many more examples. The bottom line is that

65   single phase circulation models continue to be widely used and highly useful "workhorses" in the hydrothermal community. Somewhere in the hopefully not so far future, 2-D and 3-D multi-phase models will be the new standard but for now robust and tested single-phase codes continue to be useful tools for a variety of applications.

Interestingly, even single-phase models are not that easily accessible to the hydrothermal community. Many research groups maintain 2-D research codes that resolve hydrothermal flow but single-phase 3-D models continue to be rare. To our knowledge

70   there are basically three single-phase code families that are routinely used in 3-D studies (Coumou et al., 2008; Hasenclever et al., 2014; Fontaine et al., 2014) and none of them is open-source. There are some major open-source initiatives that provide 3-D porous flow simulators or libraries such as RichardsFoam2 (Orgogozo, 2015), porousMultiphaseFoam (Horgue et al., 2015), Dumux (Flemisch et al., 2011), MRST (Lie, 2019), and OpenGeoSys (Kolditz et al., 2012) that can be used to simulate hydrothermal flow but none of them has been adapted and documented for simulating submarine hydrothermal systems. In this

75   paper, we present a toolbox, named *HydrothermalFoam*, to simulate 2-D and 3-D hydrothermal circulation in a single-phase regime for seafloor hydrothermal systems. The toolbox is build upon the open-source platform OpenFOAM® (Jasak, 1996; Weller et al., 1998), which is not only a widely used simulator for solving Navier-Stokes-type problems but also a general toolbox for solving partial differential equations. OpenFOAM is based on the cell-centroid finite volume method (FVM) and is written in C++. It provides high-level interfaces to field operations and includes a series of features such as support for flexible

80   meshes (e.g. structured meshes, unstructured meshes, and mixed meshes), utilities of pre- and post-processing, and parallel computing in 2-D and 3-D (Moukalled et al., 2016). Based on this established framework, we present a toolbox to simulate flow in submarine hydrothermal systems. We solve the porous flow problem using a continuum porous medium approach in which the fluid velocity is expressed by Darcy's law and the pressure equation is constructed from Darcy's law and the mass conservation equation. All the partial differential equations are solved implicitly in the framework of OpenFOAM and in a

85   sequential scheme, and the thermal-physical models are developed using a pure water EOS. *HydrothermalFoam* inherits all kinds of basic features of OpenFOAM, including boundary conditions. In addition, we have also customized several special boundary conditions for seafloor hydrothermal system modeling. The purpose of this toolbox is to provide the hydrothermal community with a state-of-the-art yet easy-to-use and well-documented simulator for resolving hydrothermal flow in submarine hydrothermal systems.

90   The paper is organized as follows. In section 2, we present the mathematical model, its implementation in OpenFOAM, information on initial and boundary conditions, and the thermal physical model selection. In section 3, we describe the different toolbox components, in section 4 the installation options and procedures, and in section 5 the toolbox is validated using several published benchmark tests.

Table 1. Definitions and values of variables used in this study

Symbol	Definition	Value	Unite	Variable name: OpenFOAM class
$\boldsymbol{g}$	Gravitational acceleration vector	9.81	$\mathrm{m\,s^{-2}}$	g: uniformDimensionedVectorField
T	Temperature		K	T: volScalarField
p	Pressure		Pa	p: volScalarField
k	Permeability		$\mathrm{m^2}$	permeability: volScalarField
$\boldsymbol{U}$	Darcy velocity		$\mathrm{m\,s^{-1}}$	U: volVectorField
Δt	Time step		s	deltaT_: scalar
Co	Courant number			CoNum: scalar
Co_{max}	Maximum Courant number			maxCo: scalar
$C_{\Delta t}$	Coefficient for time-step change			maxDeltaTFact: scalar
$\boldsymbol{q_h}$	Heat flux		$\mathrm{W\,m^{-2}}$	q_: scalarField
ϕ_g	Gravity related flux		$\mathrm{kg\,m^{-2}\,s^{-1}}$	
ϕ_m	Mass flux		$\mathrm{kg\,m^{-2}\,s^{-1}}$	
$\boldsymbol{n}$	Normal vector of face			
Thermal dynamic properties of fluid (IAPWS 97)				thermo: hydroThermo
C_{pf}	Specific heat of fluid		$\mathrm{m^2\,s^{-2}\,K^{-1}}$	Cp: volScalarField
μ_f	Dynamic viscosity of fluid		Pa s	mu: volScalarField
ρ_f	Density of fluid		$\mathrm{kg\,m^{-3}}$	rho: volScalarField
α_f	Thermal expansivity		$\mathrm{K^{-1}}$	alphaP: volScalarField
β_f	Compressibility		$\mathrm{Pa^{-1}}$	betaT: volScalarField
Rock properties				transportProperties:IOdictionary
ε	Porosity of rock	0.1		porosity: volScalarField
ρ_r	Density of rock	2750	$\mathrm{kg\,m^{-3}}$	rho_rock: dimensionedScalar
C_{pr}	Specific heat of rock	880	$\mathrm{J\,kg^{-1}\,K^{-1}}$	cp_rock: dimensionedScalar
k_r	Thermal conductivity of rock	1.5	$\mathrm{W\,m^{-1}\,K^{-1}}$	kr: dimensionedScalar

2 Model development

2.1 Mathematical model of hydrothermal flow

We use a continuum porous media approach and describe creeping flow in hydrothermal circulation systems using Darcy's law, where the Darcy velocity of the fluid is given by

$$\boldsymbol{U} = -\frac{k}{\mu_f}(\nabla p - \rho \boldsymbol{g}) \tag{1}$$

4

in which k denotes permeability, μ_f the fluid's dynamic viscosity, p total fluid pressure and $\boldsymbol{g}$ gravitational acceleration. All variables and symbols are listed in Table 1. Considering a compressible fluid in a porous medium with given porosity structure, the mass balance is expressed by equation (2) (Theissen-Krah et al., 2011),

$$\varepsilon \frac{\partial \rho_f}{\partial t} + \nabla \cdot (\boldsymbol{U} \rho_f) = 0 \tag{2}$$

where ε is the porosity of the rock. Note that we assume the matrix to be incompressible, so that the porosity is outside the time derivative. The equation for pressure can be derived by substituting Darcy's law (Equation 1) into the continuity equation (2) and treating the fluid's density as a function of temperature T and pressure p:

$$\varepsilon \rho_f \left(\beta_f \frac{\partial p}{\partial t} - \alpha_f \frac{\partial T}{\partial t} \right) = \nabla \cdot \left(\rho_f \frac{k}{\mu_f} (\nabla p - \rho_f \boldsymbol{g}) \right) \tag{3}$$

with α_f and β_f being the fluid's thermal expansivity and compressibility, respectively. Again there is no rock compressibilty as we consider the incomprossible matrix case. Energy conservation of a single-phase fluid can be expressed using a temperature formulation (Hasenclever et al., 2014),

$$(\varepsilon \rho_f C_{pf} + (1-\varepsilon) \rho_r C_{pr}) \frac{\partial T}{\partial t} = \nabla \cdot (k_r \nabla T) - \rho_f C_{pf} \boldsymbol{U} \cdot \nabla T + \frac{\mu_f}{k} \| \boldsymbol{U} \|^2 - \left(\frac{\partial ln \rho_f}{\partial ln T} \right)_p \left(\varepsilon \frac{\partial p}{\partial t} + \boldsymbol{U} \cdot \nabla p \right) \tag{4}$$

where C_p is heat capacity, k_r is the bulk thermal conductivity of porous rock. Subscripts of r and f refer to rock and fluid, respectively. As the matrix is incompressible, ρ_r and C_{pr} are constant in time. Fluid and rock are assumed to be in local thermal equilibrium ($T = T_r = T_f$) so that the mixture appears on the left-hand side of equation (4). Note that the assumption of thermal equilibrium is valid for most practical applications in submarine hydrothermal system modeling, as the equilibration time scale is short being related to grain size in a porous medium. However, this assumption should be carefully reviewed when simulating special geometries like fluid-filled cracks (Schmeling et al., 2018) or very short time scales like the response of a hydrothermal circulation cell to a seismic event (Wilcock, 2004). For such specialized cases OpenFOAM offers support for multi-physics models that can resolve different physics in differing parts of the modeling domain, so that heat transfer between solid and fluid can be explicitly resolved. Under the equilibrium assumption, changes in temperature depend on conductive heat transport, advective heat transport by fluid flow, heat generation by internal friction of the fluid, and pressure-volume work. Note that the third term on the righ-hand side of eqn. (4) describes viscous dissipation, while the last describes pressure-volume work (and the pressure-dependence of enthalpy, which shows up in the temperature formulation of the energy equation). Whether these terms are important depends on the application (Garg and Pritchett, 1977); our tests have shown that they matter, for example, in the pure vapor state, when simulating large vertical extents, and in supercritical states close to the critical end-point of water. All fluid properties are functions of both pressure and temperature and are calculated using the IAPWS-IF97 formulation of water and steam properties as implemented in the freesteam project (Pye, 2010). Further details on the derivation of the governing equations can be found in the appendix of Hasenclever et al. (2014).

2.2   Implemented formulation

We solve for pressure (Equation 3), velocity (Equation 1) and temperature (Equation 4) separately. Based on the finite-volume method implemented in OpenFOAM, the primary variables (p and T) related equations are discretized on an cell-centroid

computational grid. The transient temperature term in (Equation 3) is evaluated explicitly and is treated numerically as a source term resulting in a Poisson-type equation

$$\varepsilon \rho_f \beta_f \frac{\partial p}{\partial t} - \nabla \cdot \left(\rho_f \frac{k}{\mu_f} \nabla p \right) = \varepsilon \rho_f \alpha_f \frac{\partial T}{\partial t} - \nabla \cdot \left(\rho_f \frac{k}{\mu_f} \rho_f \boldsymbol{g} \right) \tag{5}$$

where the left-hand side terms are pressure transient term and Laplacian term (or diffusion term), respectively. The first term on the right-hand side is evaluated explicitly using a known temperature field, and the second term on the right-hand side is a divergence term of gravity related flux (ϕ_g), which is defined on each face of the computational grid.

To apply the finite-volume method, the advection term (the second term on the right-hand side) in the temperature equation (Equation 4) should be reformulated as a divergence term

$$\rho_f C_{pf} \boldsymbol{U} \cdot \nabla T = \nabla \cdot (\rho_f C_{pf} \boldsymbol{U} T) - T \nabla \cdot (\rho_f C_{pf} \boldsymbol{U}) \tag{6}$$

Then substituting equation (6) in equation (4), the temperature equation can be rearranged as

$$(\varepsilon \rho_f C_{pf} + (1 - \varepsilon) \rho_r C_{pr}) \frac{\partial T}{\partial t} + \nabla \cdot (\rho_f C_{pf} \boldsymbol{U} T) = \nabla \cdot (k_r \nabla T) + T \nabla \cdot (\rho_f C_{pf} \boldsymbol{U}) + \frac{\mu_f}{k} \parallel \boldsymbol{U} \parallel^2 + T \alpha_f \left(\varepsilon \frac{\partial p}{\partial t} + \boldsymbol{U} \cdot \nabla p \right) \tag{7}$$

where on the left-hand side, the first term is temperature transient term and the second one is the advection term. On the right-hand side, the first two terms represent temperature diffusion and the source term resulting from the re-formulation given in eq. (6), respectively. The last two source terms are calculated explicitly.
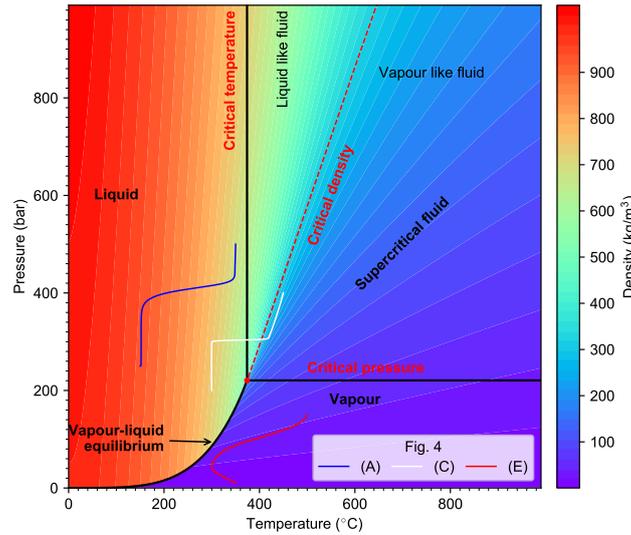
Figure 1. Phase diagram and density of pure water in temperature-pressure space. Red dot denotes supercritical point. The supercritical fluid region is outlined by critical pressure and critical temperature lines, and is divided by critical density isoline into liquid-like fluid and vapour-like fluid. Three solid curves in different colors represent pressure-temperature path of 1-D benchmark examples shown in figure 4 (A), (C) and (E), respectively.

2.3 Time-step limitations

To determine the time step, we adopt the limitation related to the Courant number Co, which is defined for compressible fluid as

$$Co = \max_{\forall cell} \left(\frac{\sum_{F=1}^{m} \phi_F}{2\rho_f V_{cell}} \right) \Delta t \tag{8}$$

with m being the number of neighbor faces to a specific cell, $\phi_F = \rho_f \boldsymbol{U} \cdot \boldsymbol{S_F}$ being mass flow through the cell faces, V_{cell} being volume of the cell and $\boldsymbol{S_f}$ being area of face F, respectively. Then the coefficient for time-step change is written as

$$C_{\Delta t} = \frac{Co_{max}}{Co} \tag{9}$$

To avoid too large changes of the time-step which could lead to numerical instabilities, the time-step is defined as follows (Jasak, 1996)

$$\Delta t = min(min(C_{\Delta t}, 1 + 0.1C_{\Delta t}), 1.2)\Delta t_{last} \tag{10}$$

where Δt_{last} is the time step length of the previous time step. Implementation details can be found in the OpenFOAM documentation and the OpenFOAM source files included by the main source code file `HydrothermalSinglePhaseDarcyFoam.C`.

2.4 Boundary conditions

To solve the pressure and temperature equations, we have to impose suitable boundary conditions for T and p. The "typical" boundary conditions, e.g. fixed value, fixed gradient and mixing of both, are directly inherited from the basic boundary conditions of OpenFOAM. In submarine hydrothermal system modeling, also some special adaptations of these basic boundary conditions can be useful.

The hydrothermal heat flux ($\boldsymbol{q_h}$) boundary condition is a fixed gradient boundary condition that is often used to approximate heat input from a crustal magma chamber and is commonly used for simulations of mid-ocean ridge hydrothermal systems (e.g. Coumou et al., 2009; Weis et al., 2014). This Neumann boundary condition is called `hydrothermalHeatFlux` in the toolbox and can be used for the temperature field. Using it, the imposed gradient of temperature can be expressed as

$$\boldsymbol{n} \cdot \nabla T = -\boldsymbol{n} \cdot \frac{\boldsymbol{q_h}}{k_r} \tag{11}$$

where $\boldsymbol{n}$ denotes the normal vector of the face boundary. In addition, we implement two options for heat flux distribution. Using the keyword `shape` allows modifying the functional form of the heat flux boundary. The available options are `fixed`, `gaussian2d`, `gaussian3d`. The default option is `fixed`, and if `gaussian2d` or `gaussian3d` is specified, the Gaussian shape (Equation 12) related parameters (`qmin, qmax, c, x0` and/or `z0`) have to be specified (see subsection 5.3).

$$q_h(x,z) = q_{min} + (q_{max} - q_{min})e^{-\frac{(x-x_0)^2 + (y-z_0)^2}{2c^2}} \tag{12}$$

A similar boundary condition called `hydrothermalMassFluxPressure` is defined for the pressure field to prescribe a mass influx into the modeling domain ($\boldsymbol{\phi_m} = \rho_f \boldsymbol{U}$). The corresponding gradient of the pressure field can be derived from

Darcy's law (Equation 1)

175 $$\boldsymbol{n} \cdot \nabla p = \boldsymbol{n} \cdot \left(\rho_f \boldsymbol{g} - \frac{\mu_f}{k} \boldsymbol{U} \right) = \frac{\mu_f}{\rho_f k} \boldsymbol{n} \cdot (\boldsymbol{\phi_g} - \boldsymbol{\phi_m}) \qquad (13)$$

Where $\boldsymbol{\phi_m}$ and $\boldsymbol{\phi_g}$ denote mass flux and gravity related flux, respectively. Further, we define another Neumann boundary condition (named `noFlux`) for the pressure field for impermeable boundaries, which is a special case of `Hydrothermal-MassFluxPressure` when $\phi_m = 0$. In addition, a Dirichlet boundary condition (named `submarinePressure`) for the pressure field is defined to describe hydrostatic pressure at the seafloor boundary due to bathymetric relief. Another commonly

180 used boundary condition on hydrothermal venting boundary (e.g. seafloor) is OpenFOAM's `inletOutlet` boundary condition, which allows to set a constant temperature for inflow and zero heat flux for outflow nodes - this type of boundary condition is often used to mimic free venting at the seafloor.

2.5 Fluid properties and equation-of-state

Numerical solutions of hydrothermal flow are known to strongly depend on the used thermodynamic properties of the simulated

185 fluid. A series of studies using realistic thermodynamic properties of pure and salt water, rather than making a Boussinesq approximation or using linearized properties, have shown that realistic results depend critically on using a realistic EOS (Jupp and Schultz, 2000; Hasenclever et al., 2014; Driesner, 2010; Carpio and Braack, 2012). Note that we here do not address any issues related to using pure versus saltwater EOSs, as outlined in the introduction. We use an EOS for pure water based on the IAPWS-IF97 parameterization and have created a corresponding OpenFOAM thermophysical model in single phase regime.

190 The phase diagram is shown in Figure 1.

2.6 Solution algorithm

The governing equations of pressure and temperature are solved in a sequential approach. The primary variables (pressure and temperature) and transport properties (such as permeability, porosity, etc.) have to be initialized before the time loop, and then the initial Darcy velocity and thermodynamic properties of fluid can be updated according to the temperature and pressure fields.

195 The main computational sequence for a single time step are described below and sketched in Figure 2.

1. The time step size Δt^{n+1} is calculated from the Courant number related condition (Equation 8).

2. Temperature field T^{n+1} is implicitly computed by solving the energy conservation equation (Equation 7). The syntax of a partial differential equation (PDE) in OpenFOAM is very close to mathematical formulation and a code snippet of the temperature equation 7 implementation is shown in listing 1. All variable symbols, names and OpenFOAM types

200 (classes) are shown in Table 1. The transient term $\partial T / \partial t$ can be implicitly discretized using the OpenFOAM operator `fvm::ddt(T)` with the discretization scheme (e.g. Euler scheme) being specified under the keyword `ddtSchemes` in the `system/fvSchemes` dictionary file (see Listing 8). The divergence term, Laplace term and source term are implicitly discretized using `fvm::div`, `fvm::laplacian` and `fvm::Sp` operators. The last term on the right-hand
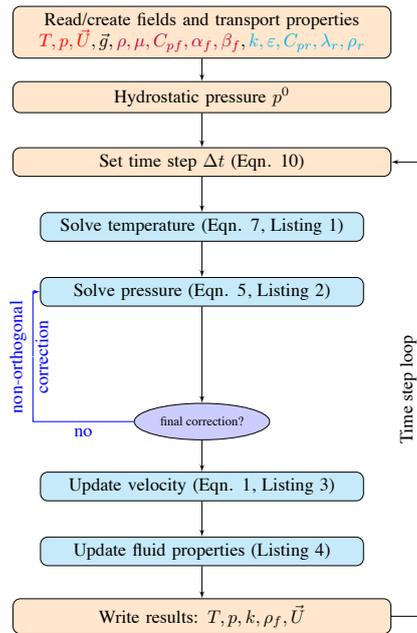
Figure 2. Schematic of the sequential algorithm.

side is explicitly calculated using known field values from the current or previous time step; the corresponding time
205   derivative and gradient can be programmed using `fvc::ddt` and `fvc::grad`, respectively.

Listing 1 Implementation of temperature equation 7 with OpenFOAM (in EEqn.H).

```
fvScalarMatrix TEqn(
    (porosity*rho*Cp+(1.0-porosity)*rho_rock*cp_rock)*fvm::ddt(T)
    +fvm::div(phi*fvc::interpolate(Cp),T)
    ==
    fvm::laplacian(kr,T) + fvm::Sp(fvc::div(phi*fvc::interpolate(Cp)),T)
    + mu/permeability*magSqr(U) + fvm::Sp(alphaP*(porosity*fvc::ddt(p)+(U &
    ↪    fvc::grad(p))),T)
);
TEqn.solve();
```

---

3. The pressure field p^{n+1} is implicitly computed by solving the pressure equation (Equation 5), the code snippet is shown in Listing 2. The temperature temporal term and divergence of ϕ_g on the right-hand side are evaluated explicitly by using `fvc::ddt(T)` and `fvc::div(phig)` (see line 7 in Listing 2). Although pressure boundary conditions are customized

by flux directly (see subsection 2.4), in order to specify pressure boundary conditions through velocity boundary conditions,

210   e.g. OpenFOAM's `fixedFluxPressure` boundary condition, the OpenFOAM's function of `constrainPressure` has to be called before solving pressure equation (see line 3 in Listing 2). For non-orthogonal mesh, a non-orthogonal correction algorithm (line 4 in Listing 2) is commonly adopted to improve accuracy for gradient computation. The number of non-orthogonal correction is specified by `nNonOrthogonalCorrectors` key in `PIMPLE` sub-dictionary in the `system/fvSolution` file.

Listing 2 Implementation of pressure equation 5 with OpenFOAM (in `pEqn.H`).

```
surfaceScalarField rhorAUf("rhorAUf", fvc::interpolate(rho*permeability/mu));
surfaceScalarField phig("phig",(fvc::interpolate(rho)*rhorAUf * g) & mesh.Sf());
constrainPressure(p, rho, U, phig, rhorAUf);
while (pimple.correctNonOrthogonal()){
    fvScalarMatrix pEqn(
        porosity*rho*betaT*fvm::ddt(p) - fvm::laplacian(rhorAUf,p)
        -porosity*rho*alphaP*fvc::ddt(T) + fvc::div(phig)
    );
    pEqn.solve();
}
```

---

215 4. The velocity field is calculated explicitly using latest pressure field based on Darcy's law (Equation 1). Instead of calculating the velocity directly, we implement an indirect approach based on OpenFOAM's function `fvc::reconstruct` to reconstruct the velocity field from the computed mass flux (see Listing 3), which performs higher numerical stability and benefits from the flux conservation characteristics of the finite volume method. In addition, boundary conditions of velocity field have to be updated (line 3 in Listing 3) if OpenFOAM's `fixedFluxPressure` boundary condition is

220   applied for pressure field.

Listing 3 Implementation of Darcy velocity calculation with OpenFOAM (in `pEqn.H`).

```
phi = phig + pEqn.flux();
U = permeability/mu*fvc::reconstruct(phi/rhorAUf);
U.correctBoundaryConditions();
```

---

5. Thermodynamic properties of fluid are updated by the thermophysical model after solving temperature and pressure field. The implementation code snippet is shown in Listing 4, in which `thermo.correct()` is used to update temperature and pressure value for all the calculating nodes. Then the thermodynamic properties of the fluid, for example density (ρ), at each nodes are calculated based on IAPWS-IF97 (see line 2-6 in Listing 4).

Listing 4 Update fluid thermo dynamic properties (in `updateProps.H`).

```
thermo.correct();
rho=thermo.rho();
mu=thermo.mu();
Cp=thermo.Cp();
alphaP=thermo.alphaP();
betaT=thermo.betaT();
```
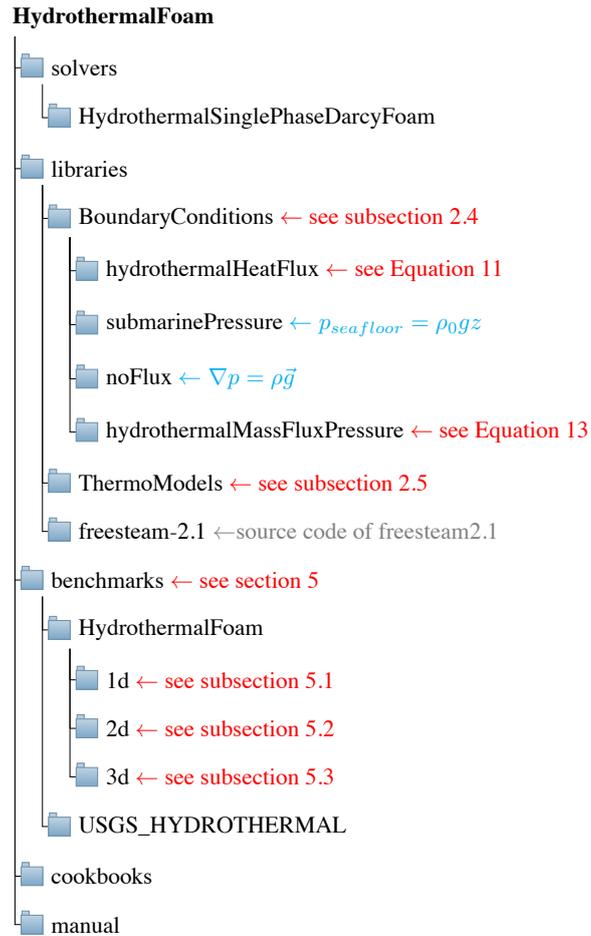
2.7 Numerical schemes

Since the numerical evaluation of the divergence and gradient terms in the governing equations has great influence on heat and mass transfer, a suitable solution strategy regarding discretization and linear solver schemes need to be chosen to ensure accuracy, robustness and stability. In the presented solver `HydrothermalSinglePhaseDarcyFoam`, the discretization and interpolation scheme of the primary fields (T, p) can be defined in the simulation configuration files. In the following benchmark tests (section 5), the advective discretization scheme is set to upwind to ensure consistency with HYDROTHERM. It should be noted that all of the basic numerical schemes of OpenFOAM are also valid for `HydrothermalSinglePhaseDarcyFoam` solver.

3 Description of toolbox components

The organization of the *HydrothermalFoam* toolbox is shown in Figure 3. The toolbox contains 5 parts: *HydrothermalFoam* solver, thermophysical models, boundary conditions, cookbooks and manual.

- `HydrothermalSinglePhaseDarcyFoam`: this block compiles the solver (an executable file) that solves the seafloor hydrothermal convection equations described in subsection 2.1. It can be used to simulate single-phase hydrothermal circulation in an isotropic porous medium.

- `ThermoModels`: this block compiles the `libHydroThermoPhysicalModels` library containing the EOS of pure water, which is used to formulate the used thermophysical model - see subsection 2.5.

- `BoundaryConditions`: this block compiles `libHydrothermalBoundaryConditions` library containing four customized boundary conditions explained in subsection 2.4. The example usage of each boundary conditions can be found in cookbooks and manual in GitLab repository (https://gitlab.com/gmdpapers/hydrothermalfoam).

- `benchmarks`: input files of all the benchmark tests (see section 5) presented in this paper.

- `cookbooks`: this block contains some example cases of parallel computing, user defined boundary conditions, and post processing.

11

HydrothermalFoam

- 📁 solvers
  - 📁 HydrothermalSinglePhaseDarcyFoam
- 📁 libraries
  - 📁 BoundaryConditions ← see subsection 2.4
    - 📁 hydrothermalHeatFlux ← see Equation 11
    - 📁 submarinePressure ← $p_{seafloor} = \rho_0 g z$
    - 📁 noFlux ← $\nabla p = \rho \vec{g}$
    - 📁 hydrothermalMassFluxPressure ← see Equation 13
  - 📁 ThermoModels ← see subsection 2.5
  - 📁 freesteam-2.1 ←source code of freesteam2.1
- 📁 benchmarks ← see section 5
  - 📁 HydrothermalFoam
    - 📁 1d ← see subsection 5.1
    - 📁 2d ← see subsection 5.2
    - 📁 3d ← see subsection 5.3
  - 📁 USGS_HYDROTHERMAL
- 📁 cookbooks
- 📁 manual

Figure 3. Structure and components of the *HydrothermalFoam* toolbox.

- – `manual`: the manual present detailed usage and all the numerical examples in cookbooks.

4 Installation

We provided two options for installation: one is building from source and the other is using a precompiled docker image.

4.1 Building from source code

4.1.1 OpenFOAM

The *HydrothermalFoam* v1.0 is developed based on OpenFOAM-7, which can be installed according to the installation instructions (https://openfoam.org/download/) given by the development team for Ubuntu Linux, Other Linux, macOS and Windows platform, respectively.

4.1.2 *HydrothermalFoam*

Once OpenFOAM is built successfully, the source code of *HydrothermalFoam* can be downloaded from Zenodo.org (Guo and Rüpke, 2020). The directory structure and components of *HydrothermalFoam* are shown in Figure 3 and the components can be built follow three steps below,

1. Build freesteam-2.1 library. The freesteam project is constructed by scons, which is a open source software construction tool dependent on python 2, and based on GSL (**G**NU **S**cientific **L**ibrary). Therefore python 2, scons and GSL have to be installed firstly, then change directory to `freesteam-2.1` in *HydrothermalFoam* source code and type command of `scons install` to compile freesteam library.

2. Build libraries of customized boundary conditions and thermophysical model. Change directory to `libraries` and type command of `./Allmake` to compile the libraries.

3. Build solver. Change directory to `HydrothermalSinglePhaseDarcyFoam` and type command of `wmake` to compile the solver.

All the library files and executable application (solver) file will be generated in directories defined by OpenFOAM's path variables of `FOAM_USER_LIBBIN` and `FOAM_USER_APPBIN`, respectively.

4.2 Precompiled docker image

In order to use all the tools directly without any compiling and development skills, we have published a precompiled Docker® image in DockerHub repository of `zguo/hydrothermalfoam`. The docker image can be used on any operation systems (e.g. Windows, Mac OS and Linux) to run *HydrothermalFoam* cases follow five steps below,

1. Install Docker, then open Docker and keep it running.

2. Pull the docker image by using command of `docker pull zguo/hydrothermalfoam` in shell terminal, e.g. bash shell in Mac OS, PowerShell in Windows system.

3. Install a container from the docker image by running shell script, e.g. Unix shell script, shown in Listing 5. The directory named `HydrothermalFoam_runs` is a shared folder between the container and host machine.

13

Listing 5 Script for installing a container from the *HydrothermalFoam* docker image.

```
dirInContainer="/home/openfoam/HydrothermalFoam_runs"
homeInHost="${1:-$HOME}"
dirInHost="${homeInHost}/HydrothermalFoam_runs"
imageName="zguo/hydrothermalfoam"
containerName="hydrothermalfoam"
docker run -it -d --name ${containerName} --workdir="/home/openfoam"
↪ -v=${dirInHost}:${dirInContainer} ${imageName}
```

4. Start the container by running command of `docker start hydrothermalfoam`.

5. Attach the container by running command of `docker attach hydrothermalfoam`. The user now in a Ubuntu linux environment with precompiled *HydrothermalFoam* tools which located at directory of `/HydrothermalFoam`. We recommend user run *HydrothermalFoam* cases in the directory of `HydrothermalFoam_runs` in the container, and then the results are synchronized in the shared directory in the host, and thus can be visualized by ParaView®, Tecplot® or other software.

Following above five steps, one can run *HydrothermalFoam* tools in the current shell terminal. Detailed instructions and five-minutes tutorial video can be found in the Docker Hub repository.
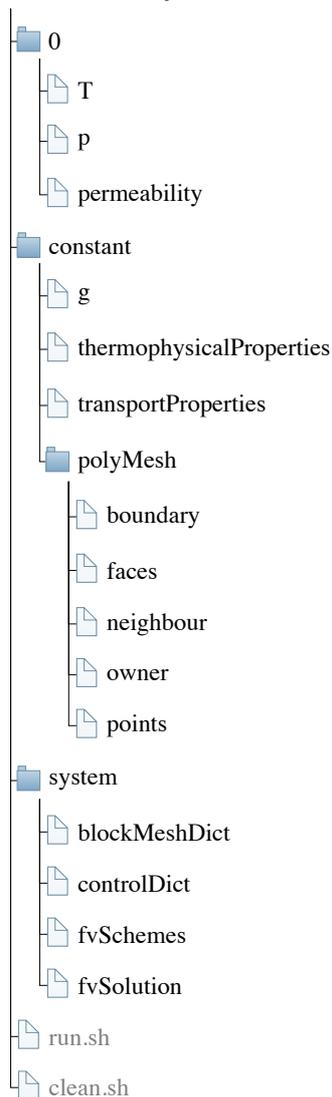
4.3 Run the first case of *HydrothermalFoam*

The basic directory structure for a *HydrothermalFoam* case, that contains the mandatory files to run an application, is shown in Figure 4. There is a bash script file named `run.sh` in every *HydrothermalFoam* cases provided by this paper. A *Hydrothermal-Foam* case can be run by executing `./run.sh`. In addition, we provide a five-minutes quick start tutorial video to run the first case of *HydrothermalFoam* in Docker.

4.3.1 Mesh generation

The mesh information containing boundary patches definitions, cell face indices and connections is located in `polyMesh` subdirectory in `constant` directory in a specific case folder (Figure 4). All the OpenFOAM mesh generation approaches can be applied to *HydrothermalFoam* as well. For example, `blockMesh` generates a simple mesh defined by `blockMeshDict` dictionary file in the `system` directory, and `gmshToFoam` transform a mesh file generated by Gmsh (Geuzaine and Remacle, 2009) to `polyMesh`.

\<Root directory of a case\>

```
├─ 📁 0
│   ├─ 📄 T
│   ├─ 📄 p
│   └─ 📄 permeability
├─ 📁 constant
│   ├─ 📄 g
│   ├─ 📄 thermophysicalProperties
│   ├─ 📄 transportProperties
│   └─ 📁 polyMesh
│       ├─ 📄 boundary
│       ├─ 📄 faces
│       ├─ 📄 neighbour
│       ├─ 📄 owner
│       └─ 📄 points
├─ 📁 system
│   ├─ 📄 blockMeshDict
│   ├─ 📄 controlDict
│   ├─ 📄 fvSchemes
│   └─ 📄 fvSolution
├─ 📄 run.sh
└─ 📄 clean.sh
```

Figure 4. Case directory structure of the *HydrothermalFoam* toolbox.

4.3.2 Input fields data

Much of the input/output data in *HydrothermalFoam* are fields, e.g. temperature, pressure data, that are read from and written into the time directories. For example, the initial time directory is commonly named 0 (see Figure 4). HydorthermalFoam writes
300   field data as dictionary files using keyword entries described in Table 2. The required input field data of *HydrothermalFoam* are temperature, pressure and permeability. Each input field data begins with an entry for its dimensions, which is expressed by

Table 2. Main keywords used in field dictionary files

Keyword	Description	Example
dimensions	Dimension of field	[0 0 0 1 0 0 0]
internalField	Value of internal field	uniform 278.15
boundaryField	Boundary field	see Listing 6

a vector of seven basic SI units (International System of Units) in order of $[kg, m, s, K, mol, A, cd]$. The file names are the same as variable names shown in Table 1. Following that, is the `internalField`, described in one of the following ways.

1. **Uniform field**. A single value is assigned to all elements within the field, taking the form:

   `internalField uniform <entry>;`

2. **Nonuniform field**. Each field element is assigned a unique value from a list, taking the form:

   `internalField nonuniform <List>;`

   The nonuniform list of internal field, e.g. permeability, can be specified in different mesh regions by using `setFields` transform `setFieldsDict` in the `system` directory (see the Heterogeneous benchmark example described in section 5.3.2).

Listing 6 Example dictionary file for temperature field `T`

```
dimensions      [0 0 0 1 0 0 0];
internalField   uniform 278.15;
boundaryField
{
    sides { type zeroGradient;}
    top { type inletOutlet; phi phi; inletValue uniform 278.15;}
    bottom { type fixedValue; value uniform 873.15;}
    frontAndBack { type empty;}
}
```

The `boundaryField` is a dictionary containing a set of entries whose names are listed in the `polyMesh/boundary` file for each boundary patches. The compulsory entry, `type`, describes the boundary condition specified for the field. Besides OpenFOAM internal basic boundary condition type of `fixedValue`, `zeroGradient`, `codedFixedValue`, et al., the customized boundary condition types, e.g. `noFlux` for pressure and `HydrothermalHeatFlux` for temperature, are described in subsection 2.4. An example set of field dictionary entries for temperature `T` are shown in Listing 6. While a

boundary condition for permeability is not mathematically required, its internal OpenFOAM datatype requires a corresponding `boundaryField` dictionary with specified boundary conditions. Therefore we suggest that the `type` entry of all boundary patches for permeability field should be always set to `zeroGradient`.

4.3.3 Thermophysical model

320 The `thermophysicalProperties` is a compulsory file in the `constant` directory, it contains keywords (Listing 7) of the new defined thermophysical model for water which is described in section 2.5 and contains constant properties of rock, e.g. porosity, density. It should be noted that porosity is implemented as `volScalarField` type just like permeability. It means that user can define porosity field in the modeling domain. If the `porosity` file doesn't exist in the start time folder, e.g. `0` folder, the solver will initialize the porosity field by the constant porosity value specified in `porousMedia` sub-dictionary in

325 `constant/thermophysicalProperties` file.

Listing 7 `thermophysicalProperties` file

```
thermoType
{
    type            htHydroThermo;
    mixture         pureMixture;
    transport       IAPWS;
    thermo          IAPWS;
    equationOfState IAPWS;
    specie          specie;
    energy          temperature;
}
mixture
{
    specie{ molWeight       18; }
    porousMedia
    {
        porosity porosity [0 0 0 0 0 0 0] 0.1;
        kr kr [1 1 -3 -1 0 0 0] 2;
        cp_rock cp_rock [0 2 -2 -1 0 0 0] 880;
        rho_rock rho_rock [1 -3 0 0 0 0 0] 2700;
    }
}
```

4.3.4 Discretized schemes and solution control

The discretization schemes for primary variables in the PDEs (Partial Difference Equations) and solver for linear equations are specified in `fvSchemes` and `fvSolution` files in `system` directory, respectively. According to implementation of temperature equation (Listing 1) and pressure equation (Listing 2), we have to specify discretization schemes for the transient terms, Laplace terms, and gradient and divergence terms, which are shown in Listing 8. A example of solver, preconditioner and tolerance settings for linear equations of temperature and pressure fields are shown in Listing 9. We recommend to keep these two files the same for different cases unless one attempts to try different options available in OpenFOAM.

5 Benchmark tests

We have conducted a number of one-dimensional (1-D), two-dimensional (2-D), and three-dimensional benchmark tests and compared the results to other established software packages to validate *HydrothermalFoam* and to highlight some of its advantages. The reference software we used is version 3.1 of HYDROTHERM, a simulation tool developed and maintained by the US Geological Survey (USGS), which can be downloaded from the internet (https://volcanoes.usgs.gov/software/hydrotherm/index.html) for free. All the parameters used in the 1-D and 2-D examples are taken from Weis et al. (2014), who presented a sequence of well-defined and highly useful benchmarks designed to test code performance within different key thermodynamic fluid states. In those benchmarks the transport properties and rock properties are constant and uniform (values are also listed in table 1); an isotropic permeability of $k = 10^{-15}\ m^2$, a porosity of $\varepsilon = 0.1$, a heat capacity of $C_{pr} = 880\,J/(kg\ ^\circ C)$, a thermal conductivity of $k_r = 2\ W/(m\ ^\circ C)$ and a rock density of $\rho_r = 2700\ kg/m^3$ are used in all simulations below.

5.1 One-dimensional simulations

We conducted six 1-D simulations to test the code performance along the three $p - T$ paths in the phase diagram of pure water shown in Figure 1. These runs are designed with constant pressure and temperature conditions on both ends of a domain with 2 km length and 10 m grid spacing. The boundary conditions and initial conditions of each 1-D test are listed in table 2. For comparison, we use the same parameters for the HYDROTHERM simulations. The computational domain is oriented horizontally (model index are A, C, E) without gravity and vertically (model index are B, D, F) with gravity to evaluate gravitational effects on fluid flow. All input files can be found in the `benchmarks/HydrothermalFoam/1d` and `benchmarks/USGS_HYDROTHERMAL/1d` directories.

Simulation results of the six 1-D examples are shown in figure 5. The example runs A and B describe invasion of a hot fluid into an initially colder domain and the fluids stay in single-phase liquid state. The thermal front moves from the start point (left or bottom for the horizontal and vertical example, respectively) towards the end point. As the vertical flow is opposing gravity, the flow is about three times slower. The fluids remain at pressures beyond the critical end point of pure water and therefore in the single-phase regime. Results calculated by HYDROTHERM and *HydrothermalFoam* are almost identical. In Examples A (horizontal) and B (vertical), the fluid remains in a liquid-like state, while in the examples C (horizontal) and

**Table 3.** Model parameters of 1-D benchmark examples

Model index	Boundary conditions		Initial conditions	End time (year)	Orientation
	left/bottom	right/top			
A	350 °C , 50 MPa	150 °C , 25 MPa	150°C , 25 MPa	250	Horizontal
B	350 °C , 50 MPa	150 °C , 25 MPa	150°C , 25 MPa	250	Vertical
C	450 °C , 40 MPa	300 °C , 20 MPa	300°C , 20 MPa	250	Horizontal
D	450 °C , 40 MPa	300 °C , 20 MPa	300°C , 20 MPa	250	Vertical
E	500 °C , 15 MPa	350 °C , 1 MPa	350°C , 1 MPa	250	Horizontal
F	500 °C , 15 MPa	350 °C , 1 MPa	350°C , 1 MPa	250	Vertical

D (vertical) the fluid is flowing along the pressure gradient from a cold liquid-like state to a hot vapor-like state. In C,D the fluids moves about two times faster than in examples A,B resulting in a sharper thermal front. The sharpness of this front is, unfortunately, often affected by the numerical scheme (e.g. mesh geometry, upwinding scheme, and advection scheme). In fact, OpenFOAM seems to cope a bit better with resolving the sharpness of the front despite also using an upwind advection scheme. Benchmarks E,F explore sub-critical vapor flow. The results of horizontal and vertical flow look very similar because density of single-phase vapor fluid is very low and thus gravitational effect are relatively small with respect to the liquid cases. The results of *HydrothermalFoam* have a good agreement with that of HYDROTHERM for single-phase vapor flow.

5.2 Two-dimensional simulations

The two-dimensional models are performed on a rectangular domain with a length of 9 km in the x-direction and 3 km in the y-direction (Figure 6), loosely representative of a vertical section through the upper oceanic crust with uniform permeability. The top boundary represents the seafloor and is kept at a constant pressure of 30 MPa, which is equivalent to about 3 km water depth and a constant temperature of 5°C. At the bottom, a constant heat flux of $Q_b = 0.05\ W/m^2$ is applied. Further, we assume a magmatic heat source with constant heat flux of $Q_m = 5\ W/m^2$ extending 1 km wide along x-direction located at the center of the bottom boundary (shown in red line in Figure 6).

The simulation results are shown in Figure 7. Fluid pressure and temperature calculated by *HydrothermalFoam* and HYDROTHERM agree very well. The evolution of the hydrothermal plume is summarized in figure (Figure 7A-C). A hot plume is forming at the base and rises upwards after 5 kyrs (Figure 7A) reaching the seafloor at 15 kyrs (Figure 7B). After 50 kyrs, a quasi-steady hydrothermal circulation cell is established (Figure 7C). The results of *HydrothermalFoam* and HYDROTHERM are again very similar. All input files can be found in the `benchmarks/HydrothermalFoam/2d` and `benchmarks/USGS_HYDROTHERMAL/2d` directories.
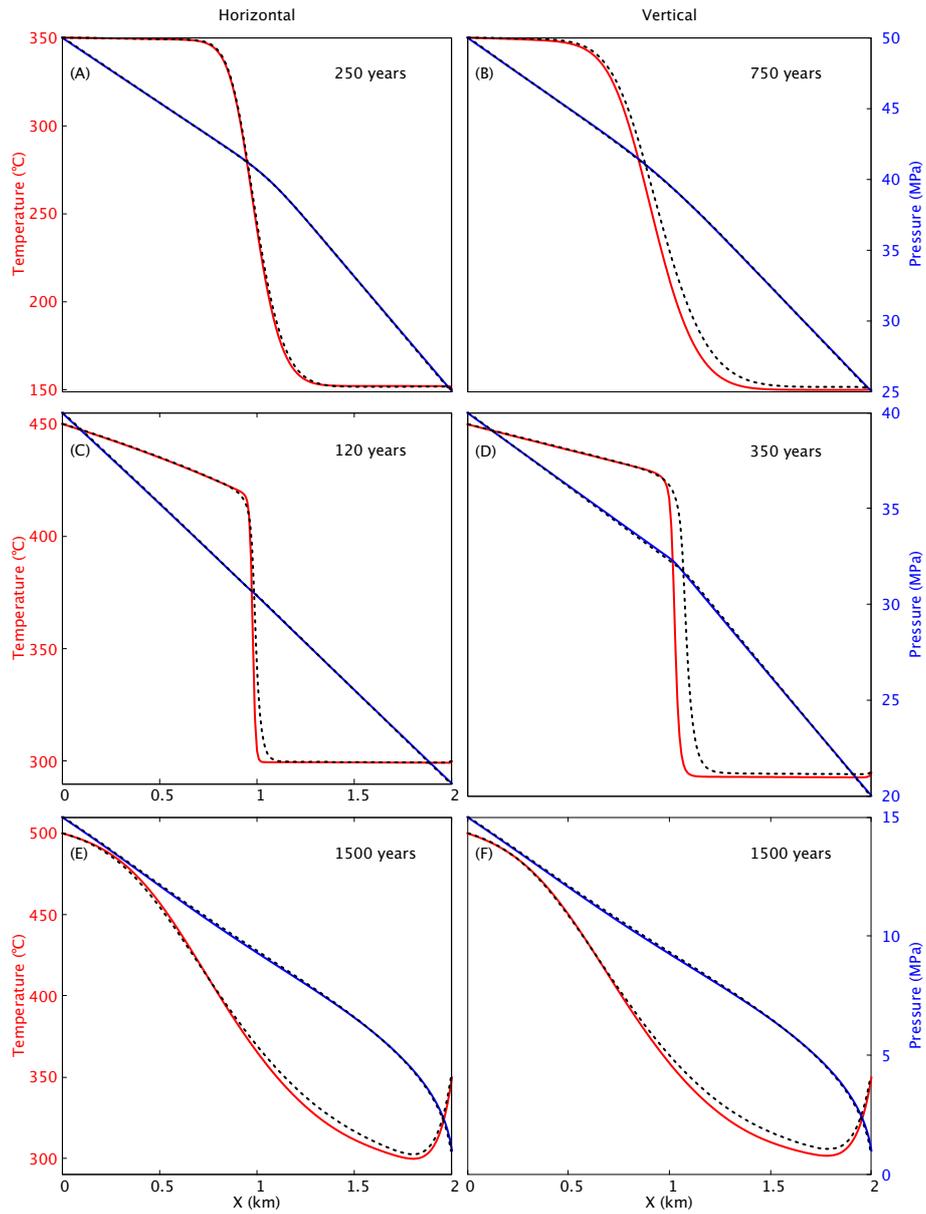
Figure 5. Snapshots of one-dimensional benchmark examples in horizontal (A, C, E) and vertical (B, D, F) orientation. Results (temperature in red and pressure in blue) of *HydrothermalFoam* and HYDROTHERM are plotted as solid lines and dashed lines, respectively.
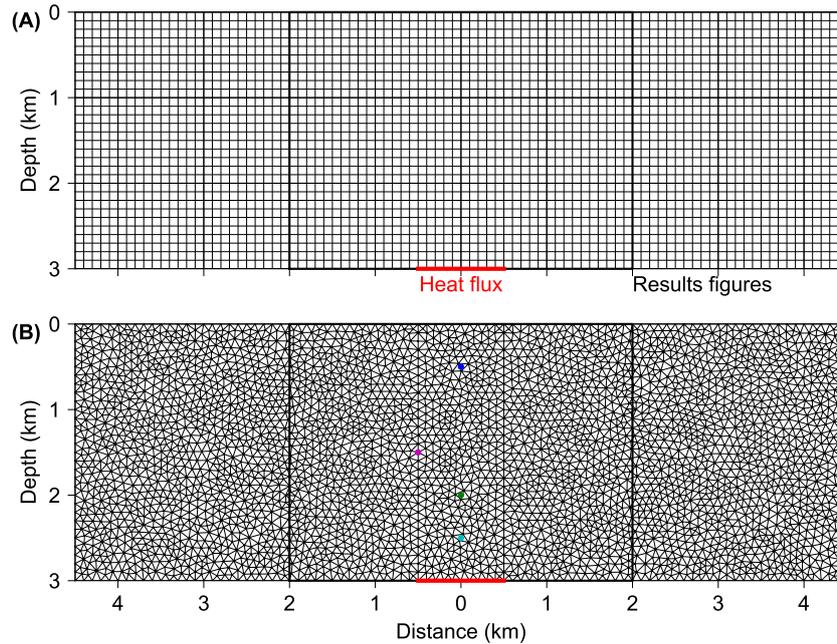
Figure 6. Mesh and model configuration of the two-dimensional examples. (A) The grid for HYDROTHERM has to be set to a uniform regular mesh with resolution of 100 m and with total number of 2700 elements. (B) *HydrothermalFoam* uses an unstructured mesh with 7074 triangular elements and the edge length in range of 60 ∼ 142 m. Red lines on the bottom boundaries denotes heat flux boundary condition for temperature.
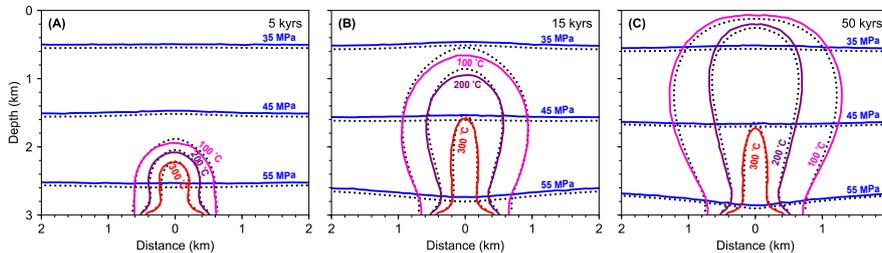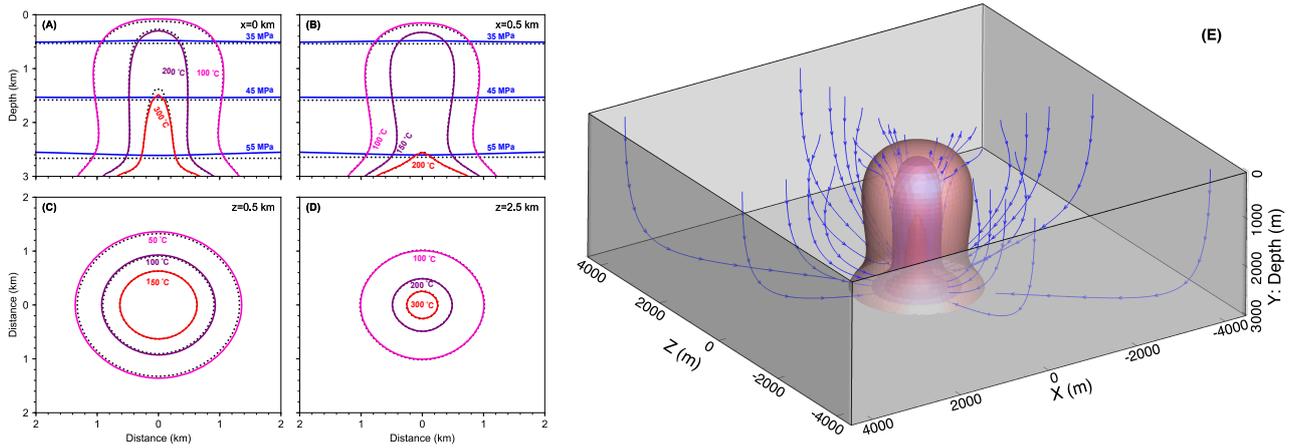

Figure 7. Snapshots of two-dimensional examples. Contour lines for fluid pressure (blue) and temperature (red) calculated from *Hydrother-malFoam* are plotted as solid lines, and that from HYDROTHERM are plotted as dotted lines (black). The visualization window is shown by the black box in Figure 6

5.3 Three-dimensional simulation

5.3.1 Homogeneous model

Similar to the two-dimensional model in subsection 5.2, the three-dimensional model are performed on a cubic domain with a
380 length of 9 km in both the x-direction and the z-direction and 3 km in y-direction (vertical direction). Note that the vertical
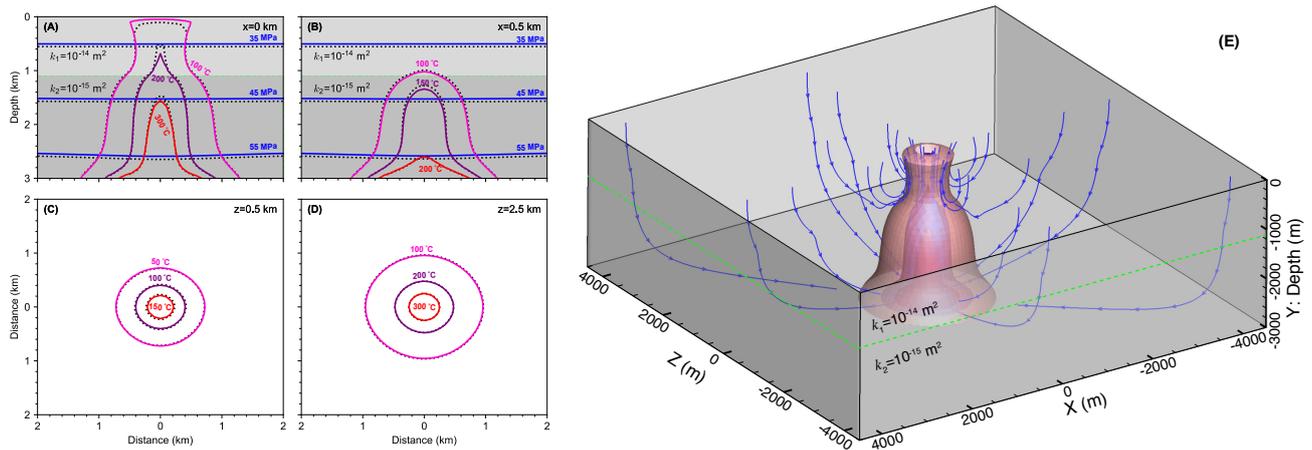
21

Figure 8. Snapshots of three-dimensional model results. Contour lines for fluid pressure (blue) and temperature calculated from *Hydrothermal-Foam* are plotted as solid lines, and that from HYDROTHERM are plotted as black dotted lines. (A) and (B) show pressure and temperature contours on vertical slices, (C) and (D) show temperature contours on horizontal slices. (E) show three-dimensional isothermal surfaces and stream lines.

coordinate in *HydrothermalFoam* or OpenFOAM is y rather than z. It can be imagined as representing a three-dimensional section of oceanic crust with uniform permeability. The top boundary is the seafloor and is kept at a constant pressure of 30 MPa and a constant temperature of 5 °C. At the bottom boundary, a zero mass flux is applied for pressure, and a constant Gaussian shaped heat flux (see Equation 12) is applied for temperature. The corresponding parameters in Equation 12

385 are $x_0 = 0, z_0 = 0, q_{max} = 5\ W/m^2, q_{min} = 0.05\ W/m^2, c = 500$. All input files can be found in the `3d/Homogeneous` directory in `benchmarks/HydrothermalFoam` and `benchmarks/USGS_HYDROTHERMAL` directories, respectively.

The simulation results at 50 kyrs are shown in Figure 8. Vertical slices at x=0 km and x=0.5 km, and horizontal slices at z=0.5 km and z=2.5 km are shown in Figure 8(A-D). Fluid pressure (blue contours) and the temperature field calculated by *HydrothermalFoam* and HYDROTHERM (dashed contours) agree very well and results on central vertical slice are very close to

390 two-dimensional model results shown in Figure 7C. Three-dimensional flow path and isothermal surfaces of 300 °C, 200 °C and 100 °C are shown in Figure 8(E).

5.3.2 Heterogeneous model

The heterogeneous model with two-layer permeability structure is modified from the homogeneous model described in subsubsection 5.3.1. Permeability of two layers are $k_1 = 10^{-14}\ m^2$ and $k_2 = 10^{-15}\ m^2$, respectively (see Figure 9 A). The

395 thickness of first layer is 1.1 km and the other parameters are the same as the homogeneous model. All input files can be found in the 3d/Heterogeneous directory in benchmarks/HydrothermalFoam and benchmarks/USGS_HYDROTHERMAL directories, respectively. The simulation results at 50 kyrs are shown in Figure 9. Vertical slices at x=0 km and x=0.5 km, and horizontal

22

Figure 9. Results of three-dimensional model with two-layer permeability structure. Two layers are separated by the green dashed line. Contour lines for fluid pressure (blue) and temperature calculated from *HydrothermalFoam* are plotted as solid lines, and that from HYDROTHERM are plotted as black dotted lines. (A) and (B) show pressure and temperature contours on vertical slices, (C) and (D) show temperature contours on horizontal slices. (E) show three-dimensional isothermal surfaces and stream lines.

slices at z=0.5 km and z=2.5 km are shown in Figure 9(A-D). The higher permeability in the upper layer results in mixing with colder ambient fluids and focussing of the upflow zone. Three-dimensional isothermal surfaces of 300 °C, 200 °C and 100 °C

400   are shown in Figure 9(E).

5.4   Cookbooks

In addition to the presented benchmarks, we have added a number of cookbooks to the code repositories that can be used as starting points for more complex models. These include simple 2-D and 3-D box models, 2-D single-pass loop models, and time-dependent permeability models. They also include examples of how to use more complex meshes generated by Gmsh

405   (Geuzaine and Remacle, 2009). We intend to add additional cookbooks in the future and hope to receive contributions from users of *HydrothermalFoam*.

6   Conclusions

We have presented a toolbox for simulating flow in submarine hydrothermal circulation systems. Being based on the widely used fluid-dynamic simulation platform OpenFOAM, the toolbox provides the user with robust parallelized 3-D solvers and a whole

410   suite of pre- and post-processing tools. The toolbox is meant to provide the interdisciplinary submarine hydrothermal systems community with an accessible and easy-to-use open-source platform for testing ideas on how hydrothermal systems 'work'. The benchmark tests have shown that model matches previously published models and the cookbooks provide the user with

23

starting points for building more sophisticated models. By following an open-source approach and by providing extensive code documentation, we hope that the presented model will facilitate integrative studies that combines models with data to better assess the role of submarine hydrothermalism in the Earth System.

Code availability.

- Program title: HydrothermalFoam

- Source code repository on GitLab: https://gitlab.com/gmdpapers/hydrothermalfoam. The latest and develop versions are maintained on this repository.

- Precompiled Docker image on Docker Hub: zguo/hydrothermalfoam. The docker image provides all the runtime environment of *HydrothermalFoam*, e.g. OpenFOAM, Gmsh, HYDROTHERM and git, users can use the *getHydrothermalFoam_latest.sh* script to fetch the latest version of *HydrothermalFoam* in the docker container.

- Five-minutes quick start tutorial video: https://youtu.be/6czcxC90gp0

- Source code documentation: https://www.hydrothermalfoam.info/doxygen

- Online manual: https://www.hydrothermalfoam.info/manual

- Licensing provision: GNU General Public License 3.0

- Programming language: C++

- Nature of problem: Seafloor hydrothermal circulation

- Solution method: The numerical approach is based on the finite-volume method (FVM).

Appendix A: Key code snippets

Author contributions. ZG, LR and CT designed the project. ZG developed the source code, ran simulations and wrote this paper. LR provided suggestions for the benchmarks and co-wrote the paper and manual. CT provided further suggestions for the manuscript and the model. All authors discussed and contributed to the final paper.

Competing interests. The authors declare that they have no conflict of interest.

24

Listing 8 Example of fvSchemes file

```
ddtSchemes
{
    default         Euler;
}
gradSchemes
{
    grad(p)         Gauss linear;
    grad(T)         Gauss linear;
}
divSchemes
{
    div(phi,T)      Gauss upwind;
    div((phi*interpolate(Cp)),T) Gauss upwind;
}
laplacianSchemes
{
    laplacian(kr,T) Gauss linear corrected;
    laplacian(rhorAUf,p) Gauss linear corrected;
}
interpolationSchemes
{
    default         linear;
}
snGradSchemes
{
    default         corrected;
}
fluxRequired
{
    default no;
    p;
}
```

Listing 9 Example of fvSolution file

```
solvers
{
    p
    {
        solver          PCG;
        preconditioner  DIC;
        tolerance       1e-12;
        relTol          0;
    }
    pFinal
    {
        $p;
        relTol          0;
    }
    T
    {
        solver          PBiCG;
        preconditioner  DILU;
        tolerance       1e-06;
        relTol          0;
    }
    "(T)Final"
    {
        $T;
        relTol          0;
    }
}
PIMPLE
{
    nNonOrthogonalCorrectors 0;
}
```

References

Andersen, C., Rüpke, L., Hasenclever, J., Grevemeyer, I., and Petersen, S.: Fault geometry and permeability contrast control vent temperatures at the Logatchev 1 hydrothermal field, Mid-Atlantic Ridge, Geology, 43, 51–54, https://doi.org/doi:10.1130/G36113.1, 2015.

Barreyre, T., Olive, J. A., Crone, T. J., and Sohn, R. A.: Depth-Dependent Permeability and Heat Output at Basalt-Hosted Hydrothermal Systems Across Mid-Ocean Ridge Spreading Rates, Geochemistry Geophysics Geosystems, 19, 1259–1281, https://doi.org/10.1002/2017gc007152, 2018.

Carpio, J. and Braack, M.: The effect of numerical methods on the simulation of mid-ocean ridge hydrothermal models, Theoretical and Computational Fluid Dynamics, 26, 225–243, https://doi.org/10.1007/s00162-011-0232-z, <GotoISI>://WOS:000298644200015, 2012.

Cathles, L. M.: A Capless 350°C Flow Zone Model to Explain Megaplumes, Salinity Variations, and High-Temperature Veins in Ridge Axis Hydrothermal Systems, Economic Geology, 88, 1977–1988, 1993.

Coumou, D., Driesner, T., and Heinrich, C. A.: The structure and dynamics of mid-ocean ridge hydrothermal systems, Science, 321, 1825–1828, https://doi.org/10.1126/science.1159582, <GotoISI>://000259501300035http://www.sciencemag.org/cgi/reprint/321/5897/1825.pdf, 2008.

Coumou, D., Driesner, T., Weis, P., and Heinrich, C. A.: Phase separation, brine formation, and salinity variation at Black Smoker hydrothermal systems, Journal of Geophysical Research: Solid Earth, 114, https://doi.org/10.1029/2008jb005764, 2009.

Crone, T. J. and Wilcock, W. S. D.: Modeling the effects of tidal loading on mid-ocean ridge hydrothermal systems, Geochemistry Geophysics Geosystems, 6, 1–25, https://doi.org/10.1029/2004gc000905, <GotoISI>://WOS:000230639200001, 2005.

Crone, T. J., Tolstoy, M., and Stroup, D. F.: Permeability structure of young ocean crust from poroelastically triggered earthquakes, Geophysical Research Letters, 38, 1–5, https://doi.org/10.1029/2011gl046820, 2011.

deMartin, B. J., Canales, R. A. R., Canales, J. P., and Humphris, S. E.: Kinematics and geometry of active detachment faulting beneath the Trans-Atlantic Geotraverse (TAG) hydrothermal field on the Mid-Atlantic Ridge, Geology, 35, 711–714, https://doi.org/10.1130/G23718A.1, 2007.

Driesner, T.: The system H2O–NaCl. Part II: Correlations for molar volume, enthalpy, and isobaric heat capacity from 0 to 1000 C, 1 to 5000 bar, and 0 to 1 XNaCl, Geochimica et Cosmochimica Acta, 71, 4902–4919, https://doi.org/10.1016/j.gca.2007.05.026, 2007.

Driesner, T.: The interplay of permeability and fluid properties as a first order control of heat transport, venting temperatures and venting salinities at mid-ocean ridge hydrothermal systems, Geofluids, 10, 132–141, https://doi.org/10.1111/j.1468-8123.2009.00273.x, <GotoISI>://WOS:000277410200010, 2010.

Driesner, T. and Heinrich, C. A.: The system H2O–NaCl. Part I: Correlation formulae for phase relations in temperature–pressure–composition space from 0 to 1000 C, 0 to 5000 bar, and 0 to 1 XNaCl, Geochimica et Cosmochimica Acta, 71, 4880–4901, https://doi.org/10.1016/j.gca.2006.01.033, 2007.

Dunn, R. A., Toomey, D. R., and Solomon, S. C.: Three-dimensional seismic structure and physical properties of the crust and shallow mantle beneath the East Pacific Rise at 9 degrees 30'N, Journal of Geophysical Research, 105, 23 537–23 555, <GotoISI>://000089895700013, 2000.

Elderfield, H. and Schultz, A.: Mid-ocean ridge hydrothermal fluxes and the chemical composition of the ocean, Annual Review of Earth and Planetary Sciences, 24, 191–224, https://doi.org/DOI 10.1146/annurev.earth.24.1.191, <GotoISI>://WOS:A1996UN64000009, 1996.

Faak, K., Coogan, L. A., and Chakraborty, S.: Near conductive cooling rates in the upper-plutonic section of crust formed at the East Pacific Rise, Earth and Planetary Science Letters, 423, 36–47, https://doi.org/10.1016/j.epsl.2015.04.025, 2015.

Flemisch, B., Darcis, M., Erbertseder, K., Faigle, B., Lauser, A., Mosthaf, K., Müthing, S., Nuske, P., Tatomir, A., Wolff, M., and Helmig, R.: DuMux: DUNE for multi-phase,component,scale,physics,... flow and transport in porous media, Advances in Water Resources, 34, 1102–1112, https://doi.org/10.1016/j.advwatres.2011.03.007, 2011.

Fontaine, F. J., Wilcock, W. S. D., Foustoukos, D. E., and Butterfield, D. A.: A Si-Cl geothermobarometer for the reaction zone of high-temperature, basaltic-hosted mid-ocean ridge hydrothermal systems, Geochemistry, Geophysics, Geosystems, 10, https://doi.org/10.1029/2009gc002407, 2009.

Fontaine, F. J., Cannat, M., Escartin, J., and Crawford, W. C.: Along-axis hydrothermal flow at the axis of slow spreading Mid-Ocean Ridges: Insights from numerical models of the Lucky Strike vent field (MAR), Geochemistry, Geophysics, Geosystems, 15, 2918–2931, https://doi.org/10.1002/2014GC005372, 2014.

Garg, S. and Pritchett, J.: On pressure-work, viscous dissipation and the energy balance relation for geothermal reservoirs, Advances in Water Resources, 1, 41–47, https://doi.org/10.1016/0309-1708(77)90007-0, 1977.

German, C. and Seyfried, W.: Hydrothermal Processes, in: Treatise on Geochemistry, pp. 191–233, Elsevier, https://doi.org/10.1016/B978-0-08-095975-7.00607-0, 2014.

German, C. R., Casciotti, K. A., Dutay, J.-C., Heimbürger, L. E., Jenkins, W. J., Measures, C. I., Mills, R. A., Obata, H., Schlitzer, R., Tagliabue, A., Turner, D. R., and Whitby, H.: Hydrothermal impacts on trace element and isotope ocean biogeochemistry, Philosophical Transactions of the Royal Society A: Mathematical, Physical and Engineering Sciences, 374, 20160035, https://doi.org/10.1098/rsta.2016.0035, 2016.

Germanovich, L. N., Lowell, R. P., and Astakhov, D. K.: Stress-dependent permeability and the formation of seafloor event plumes, Journal of Geophysical Research: Solid Earth, 105, 8341–8354, https://doi.org/10.1029/1999jb900431, 2000.

Geuzaine, C. and Remacle, J.-F.: Gmsh: A 3-D finite element mesh generator with built-in pre-and post-processing facilities, International journal for numerical methods in engineering, 79, 1309–1331, https://doi.org/10.1002/nme.2579, 2009.

Grevemeyer, I., Hayman, N. W., Lange, D., Peirce, C., Papenberg, C., Van Avendonk, H. J. A., Schmid, F., de La Peña, L. G., and Dannowski, A.: Constraining the maximum depth of brittle deformation at slow- and ultraslow-spreading ridges using microseismicity, Geology, 47, 1069–1073, https://doi.org/10.1130/g46577.1, 2019.

Guo, Z. and Rüpke, L.: HydrothermalFoam v1.0, https://doi.org/10.5281/zenodo.3755647, 2020.

Hannington, M., Jamieson, J., Monecke, T., Petersen, S., and Beaulieu, S.: The abundance of seafloor massive sulfide deposits, Geology, 39, 1155–1158, https://doi.org/10.1130/g32468.1, 2011.

Hasenclever, J., Theissen-Krah, S., Rüpke, L. H., Morgan, J. P., Iyer, K., Petersen, S., and Devey, C. W.: Hybrid shallow on-axis and deep off-axis hydrothermal circulation at fast-spreading ridges, Nature, 508, 508–512, https://doi.org/10.1038/nature13174, 2014.

Horgue, P., Soulaine, C., Franc, J., Guibert, R., and Debenest, G.: An open-source toolbox for multiphase flow in porous media, Computer Physics Communications, 187, 217–226, https://doi.org/10.1016/j.cpc.2014.10.005, 2015.

Ingebritsen, S., Geiger, S., Hurwitz, S., and Driesner, T.: Numerical simulation of magmatic hydrothermal systems, Reviews of Geophysics, 48, https://doi.org/10.1029/2009RG000287, 2010.

Jamieson, J. W., Clague, D. A., and Hannington, M. D.: Hydrothermal sulfide accumulation along the Endeavour Segment, Juan de Fuca Ridge, Earth and Planetary Science Letters, 395, 136–148, https://doi.org/10.1016/j.epsl.2014.03.035, 2014.

Jasak, H.: Error analysis and estimation for the finite volume method with applications to fluid flows., Ph.D. thesis, Imperial College of Science, Technology and Medicine, https://spiral.imperial.ac.uk/bitstream/10044/1/8335/1/Hrvoje_Jasak-1996-PhD-Thesis.pdf, 1996.

Jupp, T. and Schultz, A.: A thermodynamic explanation for black smoker temperatures, Nature, 403, 880–883, https://doi.org/10.1038/35002552, 2000.

Jupp, T. E. and Schultz, A.: Physical balances in subseafloor hydrothermal convection cells, Journal of Geophysical Research-Solid Earth, 109, https://doi.org/10.1029/2003jb002697, <GotoISI>://WOS:000221911900002, 2004.

Kipp, K. L., Hsieh, P. A., and Charlton, S. R.: Guide to the Revised Ground-Water Flow and Heat Transport Simulator: HYDROTHERM– Version 3, US Department of the Interior, US Geological Survey, http://pubs.usgs.gov/tm/06A25/, 2008.

Kolditz, O., Bauer, S., Bilke, L., Böttcher, N., Delfs, J.-O., Fischer, T., Görke, U. J., Kalbacher, T., Kosakowski, G., McDermott, C., et al.: OpenGeoSys: an open-source initiative for numerical simulation of thermo-hydro-mechanical/chemical (THM/C) processes in porous media, Environmental Earth Sciences, 67, 589–599, https://doi.org/10.1007/s12665-012-1546-x, 2012.

Lewis, K. and Lowell, R.: Numerical modeling of two-phase flow in the NaCl-H2O system: Introduction of a numerical method and benchmarking, Journal of Geophysical Research: Solid Earth, 114, https://doi.org/10.1029/2008JB006029, 2009a.

Lewis, K. and Lowell, R.: Numerical modeling of two-phase flow in the NaCl-H2O system: 2. Examples, Journal of Geophysical Research: Solid Earth, 114, https://doi.org/10.1029/2008JB006029, 2009b.

Lie, K.-A.: An introduction to reservoir simulation using MATLAB/GNU Octave : user guide for the MATLAB Reservoir Simulation Toolbox (MRST), Cambridge University Press, https://doi.org/10.1017/9781108591416, https://doi.org/10.1017/9781108591416, 2019.

Lister, C. R. B.: Penetration of water into hot rock, Geophysical Journal of the Royal Astronomical Society, 39, 465–509, https://doi.org/10.1111/j.1365-246X.1974.tb05468.x, 1974.

Lowell, R. P.: Modeling continental and submarine hydrothermal systems, Reviews of Geophysics, 29, 457–476, https://doi.org/10.1029/91rg01080, 1991.

Lowell, R. P., Farough, A., Germanovich, L. N., Hebert, L. B., and Horne, R.: A Vent-Field-Scale Model of the East Pacific Rise 9 degrees 50 ' N Magma-Hydrothermal System, Oceanography, 25, 158–167, <GotoISI>://WOS:000301095200016, 2012.

Middleton, J. L., Langmuir, C. H., Mukhopadhyay, S., McManus, J. F., and Mitrovica, J. X.: Hydrothermal iron flux variability following rapid sea level changes, Geophysical Research Letters, 43, 3848–3856, https://doi.org/10.1002/2016gl068408, 2016.

Moukalled, F., Mangani, L., Darwish, M., et al.: The finite volume method in computational fluid dynamics, vol. 113, Springer, https://doi.org/10.1007/978-3-319-16874-6_21, 2016.

Olive, J. A. and Crone, T. J.: Smoke Without Fire: How Long Can Thermal Cracking Sustain Hydrothermal Circulation in the Absence of Magmatic Heat?, Journal of Geophysical Research-Solid Earth, 123, 4561–4581, https://doi.org/10.1029/2017jb014900, 2018.

Orgogozo, L.: RichardsFoam2: A new version of RichardsFoam devoted to the modelling of the vadose zone, Computer Physics Communications, 196, 619 – 620, https://doi.org/https://doi.org/10.1016/j.cpc.2015.07.009, http://www.sciencedirect.com/science/article/pii/S0010465515002787, 2015.

Pruess, K., Oldenburg, C., and Moridis, G.: TOUGH2 user's guide, version 2.1. Earth sciences division, Lawrence Berkeley National Laboratory University of California, Berkeley, California (USA), https://www.osti.gov/biblio/751729-tough2-user-guide-version, 1999.

Pye, J.: Freesteam project, https://sourceforge.net/projects/freesteam/, 2010.

Schlindwein, V. and Schmid, F.: Mid-ocean-ridge seismicity reveals extreme types of ocean lithosphere, Nature, 535, 276–279, https://doi.org/10.1038/nature18277, 2016.

Schmeling, H., Marquart, G., and Grebe, M.: A porous flow approach to model thermal non-equilibrium applicable to melt migration, Geophysical Journal International, 212, 119–138, https://doi.org/10.1093/gji/ggx406, 2018.

Singh, S. and Lowell, R. P.: Thermal response of mid-ocean ridge hydrothermal systems to perturbations, Deep Sea Research Part II: Topical Studies in Oceanography, 121, 41–52, https://doi.org/10.1016/j.dsr2.2015.05.008, 2015.

Stein, A. and Stein, S.: Constraints on hydrothermal heat flux through the oceanic lithosphere from global heat flow, Journal of Geophysical Research, 99, 3081–3095, 1994.

Tagliabue, A., Bopp, L., Dutay, J. C., Bowie, A. R., Chever, F., Jean-Baptiste, P., Bucciarelli, E., Lannuzel, D., Remenyi, T., Sarthou, G., Aumont, O., Gehlen, M., and Jeandel, C.: Hydrothermal contribution to the oceanic dissolved iron inventory, Nature Geoscience, 3, 252–256, https://doi.org/10.1038/Ngeo818, <GotoISI>://WOS:000276159600015, 2010.

Tao, C., Seyfried, W. E., J., Lowell, R. P., Liu, Y., Liang, J., Guo, Z., Ding, K., Zhang, H., Liu, J., Qiu, L., Egorov, I., Liao, S., Zhao, M., Zhou, J., Deng, X., Li, H., Wang, H., Cai, W., Zhang, G., Zhou, H., Lin, J., and Li, W.: Deep high-temperature hydrothermal circulation in a detachment faulting system on the ultra-slow spreading ridge, Nat Commun, 11, 1300, https://doi.org/10.1038/s41467-020-15062-w, 2020.

Theissen-Krah, S., Iyer, K., Rüpke, L. H., and Morgan, J. P.: Coupled mechanical and hydrothermal modeling of crustal accretion at intermediate to fast spreading ridges, Earth and Planetary Science Letters, 311, 275–286, 2011.

Theissen-Krah, S., Rüpke, L. H., and Hasenclever, J.: Modes of crustal accretion and their implications for hydrothermal circulation, Geophysical Research Letters, 43, 1124–1131, https://doi.org/10.1002/2015GL067335, 2016.

Vehling, F., Hasenclever, J., and Rüpke, L.: Implementation Strategies for Accurate and Efficient Control Volume-Based Two-Phase Hydrothermal Flow Solutions, Transport in Porous Media, 121, 233–261, https://doi.org/10.1007/s11242-017-0957-2, 2018.

Weis, P., Driesner, T., Coumou, D., and Geiger, S.: Hydrothermal, multiphase convection of H2O-NaCl fluids from ambient to magmatic temperatures: a new numerical scheme and benchmarks for code comparison, Geofluids, 14, 347–371, https://doi.org/10.1111/gfl.12080, 2014.

Weller, H. G., Tabor, G., Jasak, H., and Fureby, C.: A tensorial approach to computational continuum mechanics using object-oriented techniques, Computers in physics, 12, 620–631, https://doi.org/10.1063/1.168744, 1998.

Wilcock, W. S. D.: Physical response of mid-ocean ridge hydrothermal systems to local earthquakes, Geochemistry, Geophysics, Geosystems, 5, n/a–n/a, https://doi.org/10.1029/2004gc000701, 2004.

Zyvoloski, G. A., Robinson, B. A., Dash, Z. V., and Trease, L. L.: Summary of the models and methods for the FEHM application-a finite-element heat-and mass-transfer code, Tech. rep., Los Alamos National Lab., NM (US), https://www.osti.gov/biblio/14903, 1997.